Hindawi
Journal of Nanomaterials
Volume 2022, Article ID 3864758, 13 pages
https://doi.org/10.1155/2022/3864758

Research Article

Biogenic Silver Nanoparticles Fabricated by *Euphorbia granulata* Forssk's Extract: Investigating the Antimicrobial, Radical Scavenging, and Catalytic Activities

Govindasami Periyasami,[1] **Selvakumar Palaniappan**,[2] **Ponmurugan Karuppiah**,[3] **Mostafizur Rahaman**,[1] **Perumal Karthikeyan**,[4] **Ali Aldalbahi**,[1] **and Naif Abdullah Al-Dhabi**[3]

[1]*Department of Chemistry, College of Science, King Saud University, Riyadh-11451, Saudi Arabia*
[2]*Department of Food Science and Postharvest Technology, Haramaya Institute of Technology, Haramaya University, Dire Dawa-P.O. Box 138, Ethiopia*
[3]*Department of Botany and Microbiology, College of Science, King Saud University, Riyadh-11451, Saudi Arabia*
[4]*Department of Chemistry and Biochemistry, Ohio State University, 170A CBEC, 151 Woodruff Avenue, Columbus, Ohio 43210, USA*

Correspondence should be addressed to Govindasami Periyasami; pkandhan@ksu.edu.sa
and Selvakumar Palaniappan; selva.kumar@haramaya.edu.et

Received 19 January 2022; Revised 16 February 2022; Accepted 1 March 2022; Published 11 April 2022

Academic Editor: Mazeyar Parvinzadeh Gashti

The plants of Euphorbiaceae have high medicinal values and their phytochemical composition plays a major role in metal ion reduction. In this research, *Euphorbia granulata* (EG) the "spurge family" plant extract was used to reduce silver ions to silver nanoparticles (AgNPs). This nanoparticle formation was observed by UV-VIS spectrophotometric analysis at different times and temperatures to achieve the most optimal conditions. The synthesized biogenic silver nanoparticles (EG-AgNPs) were subjected to FTIR studies. The obtained low-intensity bands of fingerprint region bands (612 cm^{-1}) and aromatic OH bands (3385 cm^{-1}) are identified that the reduction of silver ions (Ag^{+}) into metallic silver (Ag^{0}) nanoparticles. Further, the charge, size, and morphology of the synthesized EG-AgNPs were studied using various spectroscopic methods including powder X-ray diffraction (XRD), high-resolution scanning electron microscope (HRSEM), FESEM-EDX elemental mapping, and high-resolution transmission electron microscope (HRTEM). The notable efficacy of the EG-AgNPs in antimicrobial activity including minimum inhibitory concentration (MIC) and minimum bactericidal concentration (MBC) suggested the EG-AgNPs are noteworthy material for biomedical applications. EG-AgNPs exhibited an efficient photocatalytic activity by degrading environmental pollutants, methylene blue (MB), and methyl orange (MO) dyes. The antioxidant property by radical scavenging (DPPH) assay of synthesized AgNPs was studied. Furthermore, the studied antioxidant behavior of EG-AgNPs by DPPH assay strongly supports that the EG-AgNPs are highly suitable materials for anticancer agents.

1. Introduction

Phytogenic metal nanoparticles have privileged status in nanoscience and nanotechnology research due to their innovative nature such as unique size, shape, and reduced dimensions. Over the last few decades, metal nanoparticles have been explored much in various research fields including medicinal, optical, and catalytic activities [1]. The literature reports showed that the notable properties and activities of nanoparticles are completely dependent on their size, shape,

morphology, and distribution [2]. Particularly, size and shape of the particles are playing determinative roles in achieving adequate results in biomedical applications [3, 4]. Such unique particles can be prepared by employing plant extract prompted synthetic methods [5].

Due to its noteworthy physical, chemical, and biological properties, silver nanoparticles (AgNPs) are showing superlative applications in medicinal chemistry including cancer therapy, biotechnology, and water treatment depending on their particle size [6]. Recently, our research group reported that the biosorbed AgNPs are used as food packing materials composite due to their high efficacy antimicrobial activity [7]. Among the various availed synthetic routes, environmentally benign green synthetic methodology is an ecofriendly alternative to save the globe and human health from toxic chemical synthetic methods [8]. Also, using natural resources, such as plants including fruits, barks, roots, seeds, rhizomes, leaves, agrifood waste, and by-products to prepare metal nanoparticles is an emergent concern towards cheaper and cost effective [9]. Unlike plants, bacteria and fungi chemical and physical methods require relatively long incubation times and triggering biosafety issues while reduction of metal ions, the medicinal plants extract-mediated reduction of metal ions, is more stable and cost effective [10].

Also, using such plant extract green synthetic methods is a beneficial method to achieve large-scale biogenic AgNPs without any toxic by-products. So, it is the responsibility of world researchers to reduce the production of toxic residues and encouraged to develop harmless and highly sustainable methods like green synthetic methods of nanoparticles. The employed plant extract contain biodegradable antioxidant biocomponents including phenols, phenolic polysaccharides, proteins, and vitamins that play simultaneously both reduction of metal ions and stabilization of nanoparticles [11]. Also, the interesting feature of this green methodology is, despite the fluctuating concentration of biocomponents depending on aging of the natural product and differing from growing environment, the most relevant reducing compounds remains in high concentration to reduce the metal ions [12].

The present work focuses on the development of colloids of AgNPs mediated with *Euphorbia granulata* Forssk. and studies the *in vitro* biological applications. The synthesis and stabilization of biogenic AgNPs (EG-AgNPs) will be achieved by employing unreported *E. granulata* plant extract, which is a widely existing weed plant in dried area including Saudi Arabian Peninsula and central Asia. *E. granulata* (EG) belongs to Euphorbiaceae family and contains a considerable amount of phenolic and flavonoid compounds and possessing antioxidant capacity. The schematic diagram of the scope of the proposed work is presented in Figure 1.

2. Materials and Methods

2.1. Plants and Chemicals. The *Euphorbia granulata* Forssk. plant was collected from King Saud University premises, Riyadh, and identified (No. 22521) by Dr. Rajagopalan from the Department of Botany and Microbiology, Herbarium division, King Saud University, Riyadh, Saudi Arabia, and

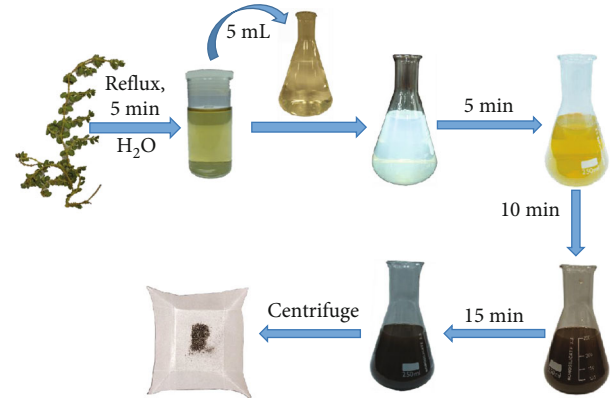

Figure 1: Schematic diagram of synthesis of *E. granulata* plant extract supported biogenic synthesis of AgNPs.

was identified as the plant specimen. The collected fresh plant was washed thoroughly in running water and further rinsed with deionized water. All the chemicals that were used in the experiments are of analytical grade. Silver nitrate ($AgNO_3$, Sigma-Aldrich) was purchased and used as received. For the antimicrobial studies, nutrient agar, Muller-Hinton agar, ciprofloxacin, and amphotericin were purchased from HiMedia, India, and used as received.

2.2. Preparation of Plant Extract and Characterization. The plant extraction was collected from boiled milli-Q water by the general procedure. Typically, 10 g of the cleaned plant was chopped into small pieces using mortar and pestle and subjected for extraction with 500 mL of milli-Q water in an Erlenmeyer flask. The mixture was boiled 5 min, and then, the extract was decanted. The decanted crude extract was further filtered using Whatman no. 1 filter paper up to the extract is clear solution and then stored at 4°C for further use. The UV spectrum of *E. granulata* plant extract was recorded and observed the absorption bands between 250 and 400 nm. This wide range of absorption was comprised of multiple peaks due to the presence of multiple phytochemical compositions in the extract instead of the finely resolved peak like flavonoids (325 nm), tannins (280 nm), quercetins (255 and 366 nm), and phenolics (255 and 365 nm) [13].

2.3. Qualitative Phytochemical Analysis. Qualitative phytochemical analysis of the *E. granulata* extract was performed using the standard experimental procedures to observe the common phytoconstituents. Among the existing phytocomponents in the *E. granulata* extract, phenolic/polyphenolic compositions were analyzed by lead acetate and alkaline reagent test. Also, the presence of flavonoids was analyzed by adopting Shinoda alkaline reagent. All the experiments for quantitative phytochemical analysis were done in triplicates. The observed antioxidant compositions in the plant extract were indicated qualitatively as positive (+) or negative (−).

2.3.1. Total Phenolic Content (TPC) Determination. The Folin-Ciocalteu (F-C) assay involved finding out the antioxidant capacity of natural product components by a single-electron transfer mechanism. Moreover, like 2,2′-azinobis-

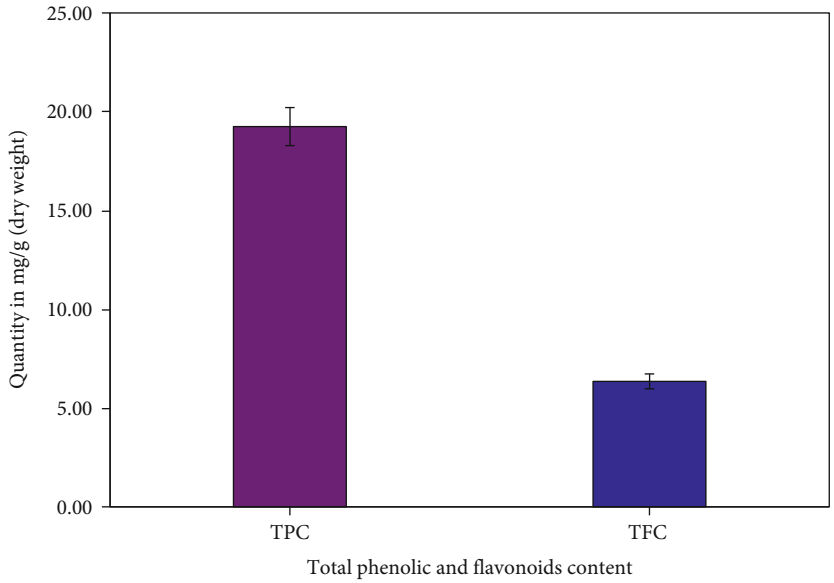

Figure 2: Total phenolic and flavonoids content of aqueous extract of *E. granulata*.

Table 1: Qualitative screening for phytochemical constituents of *E. granulata* aqueous extract.

Phytochemical constituents	Obtained components[$]
Alkaloids	+
Tannins	+
Glycoside	+
Phenolic compounds	+++
Flavonoids	++
Carbohydrates	+
Proteins	+
Triterpenoids	+
Steroids and sterols	—
Saponins	—
Anthraquinones	—

[$]"+": present, "-": absent.

3-ethylbenzothiazoline-6-sulfonic acid (ABTS) assay, the F-C method was also useful for assaying compounds of biomedical interest for antioxidant activity. Therefore, the F-C method was utilized to determine the presence of phenolic contents as well as other aromatic OH components [14], Totally, 10 mL of reaction mixture prepared by mixing of 1 mL plant extract, 5 mL F-C reagent, and 4 mL of 7% Na_2CO_3. The mixture was incubated 30 min in 40°C water bath. Then, the OD observation was expressed as gallic acid equivalents present per mg of the plant extract. The TPC was determined using UV-Vis double beam spectrophotometer and based on the obtained triplicate values. The amount of TPC in the plant extracts was calculated by using the formula:

$$\text{TPC} = C1 \times \frac{V}{m}, \quad (1)$$

where TPC is in mg/g of gallic acid equivalent, $C1$ is concentration of gallic acid (mg/m), V is volume of extract solution (mL), and m is the weight of the plant extract (g).

2.3.2. Total Flavonoid Content (TFC) Determination. The presence of flavonoids was determined by amended aluminum chloride colorimetric method [15]. Typically, 1 mL of plant extract was mixed with 3 mL of analytically pure methanol, and then, 0.1 mL of AlCl3 (10%) and 0.1 mL of 1 M CH_3COOK was added and diluted with 3 mL of distilled water and incubated 30 min at ambient temperature. Then, the OD of the mixture was measured and absorbance results in the presence of flavonoids in terms of quercetin equivalent, as a standard. The TFC was determined as mg/g of quercetin equivalent of EG materials in the triplicate value.

The measurement was carried out in the triplicate value based on the quercetin equivalent of EG extract, and the TFC in the plant extract was calculated by using following formula:

$$\text{TFC} = C1 \times \frac{V}{m}, \quad (2)$$

where TFC is in mg/g of quercetin equivalent, $C1$ is concentration of quercetin (mg/L), V is volume of extract solution (mL), and m is the weight of the plant extract (g).

2.4. Biological Studies of EG-AgNPs

2.4.1. Antimicrobial Activity of EG-AgNPs. The antimicrobial activity of biosynthesized EG-AgNPs were determined with six bacterial and two fungal strains including *Staphylococcus aureus* (ATCC 25923), *Escherichia coli* (ATCC 25922), *Listeria monocytogenes* (ATCC 51779), *Pseudomonas aeruginosa* (ATCC 39327), *Klebsiella pneumoniae* (ATCC 4352), *Enterococcus faecalis* (ATCC 29212), *Candida albicans* (ATCC 10231), and *Cryptococcus* sp. (ATCC MYA 1763)

were obtained from King Khalid University Hospital, Riyadh, Saudi Arabia. The antimicrobial activity of biosynthesized EG-AgNPs was assessed with agar well diffusion methods (CLSI, 2020) [13]. For enhanced diffusion, Muller-Hinton agar (MHA) was used and wells (6.0 mm) were made on plates with a sterile cork-borer. The bacterial strains were cultured after realizing a turbidity of 0.5 McFarland standard on each plate using a sterile swab. Following, different concentrations (15, 25, 50, and 75 μg/mL) of EG-AgNP solution were transferred into each well, and the plates were incubated at 37°C for 24 h. Earlier, the biosynthesized AgNPs were prepared at the concentration of 1 mg/mL with dimethyl sulfoxide (DMSO). The inhibition zone diameter (mm) was measured after the incubation. Ciprofloxacin, amphotericin, and sterilized distilled H_2O used as positive and negative controls, respectively. The experiments were completed in triplicates, and the results were presented in terms of mean standard deviation [16].

2.4.2. Determination of Minimum Inhibitory Concentration (MIC) and Minimum Bactericidal Concentration (MBC). Biosynthesized EG-AgNP solution was prepared in sterile 96-well plates by twofold serial dilution in the range of 0.78–100 μg/mL for determining MIC and MBC. The wells were then inoculated with 18 h bacterial strains and adjusted to 0.5 McFarland, diluted at a 1 : 100 ratio, and then incubated at 37°C for 18 h. Later, the MIC values were determined with a microtiter plate reader (Bio-Rad Laboratories, USA) at 600 nm. The MBC was determined through the spreading of broth from the nongrowth wells onto nutrient agar plates and was incubated at 37°C for 24 h. MBC was differentiated based on the concentration without any growth of the bacterial strains [17].

2.5. Determination of Radical Scavenging Activity of by DPPH Method. The antioxidant radical scavenging activity was determined with the 1,1-diphenyl-2-picrylhydrazil (DPPH) radical scavenging assay method described by Okawa et al. [18]. A 100 mL of 0.01 mmol concentration DPPH solution was prepared by 3.94 g of DPPH in 100 mL methanol at room temperature. The optical density (OD) of DPPH was optimized at 1.0 (±0.02) at 520 nm by adjusting the concentration of DPPH solution. 1 mL of plant extract was mixed with 1 mL of 1.0 mmol DPPH solution followed by incubation at room temperature for 30 minutes. The OD of the prepared solution was taken at optimized nanometer, and the results were expressed in percentage of radical scavenging activity using ascorbic acid (ACA) as the standard. The scavenging ability was calculated by using following formula:

$$\text{Inhibition\%} = \left\{ \frac{\lambda \text{ control} - \lambda \text{ sample}}{\lambda \text{ control}} \right\} \times 100. \quad (3)$$

2.6. Photocatalytic Activity of EG-AgNPs. Water contaminations particularly organic dyes are extremely threatening as carcinogenic and mutagenic agents to humans. Therefore, it is highly important to remove harmful dyes from wastewater and industrial effluents. Methyl orange (MO), Methylene blue (MB), Rose Bengal (RB), and Congo Red (CR) are well-known organic dyes that are major wastewater contaminations. In the present study, the photocatalytic degradation of anionic contaminant MO and cationic contaminant MB dyes was carried out using synthetized EG-AgNPs as a degradation catalyst [19]. The process was carried out under the sunlight and UV light irradiation; then, the absorption was monitored using a UV spectrophotometer. Initially, 100 mL of EG-AgNP homogeneous solution was prepared by adding 20 mg of nanocatalyst in 100 mL milli-Q water by sonicating 10 min with 20 Hz amplification. The resulting homogeneously dispersed nanocatalyst solution was used for the experiments.

For the degradation study, 50 mL of 1 mmol MO and MB solutions were prepared and UV absorption of the dye solutions was measured as 424 nm and 668 nm for the MO and MB dyes, respectively. In each experiment, with each 50 mL of aqueous dye solution, 10 mL of homogeneously dispersed nanocatalyst solution was added in dark condition, and the absorption was recorded at 0 min of nanocatalyst addition. The reaction was investigated under sunlight and UV light exposer, and the absorption was reordered periodically using a UV-visible spectrophotometer. The percentage of dye degradation was calculated using the following equation:

$$DP(t) = \left\{ \frac{(A0 - At)}{A0} \right\} \times 100, \quad (4)$$

where A_0 is initial absorption and A_t is recorded absorption periodically of the dye solution. The experiment was completed in triplicate.

3. Results and Discussion

3.1. Characterization Methods of Synthesizing EG-AgNPs. The bioextract-mediated reduction of silver ions (Ag^+) into silver nanoparticles (Ag^0) was monitored in an aqueous solution by a UV-Vis spectrophotometer (Spectra UV-VIS double beam UVD-3500, Labomed, Inc.) at regular time interval in wavelength ranges between 200 and 800 nm at room temperature. One equivalent of reaction mixture was diluted with 3 equivalent volume of deionized water, and the absorption was measured. The synthesized biosorbed EG-AgNPs were subjected to Fourier transform infrared spectroscopy (FTIR) analysis to identify the presence of functional groups. The FTIR was performed using Fourier transform infrared spectrophotometer, Shimadzu with a resolution of 4 cm^{-1}. The samples were scanned in the spectral ranges of 4,000–500 cm^{-1} by an average of 25 scans per sample, and the result obtained was analyzed. Properly washed and dried sample of synthesized EG-AgNPs was used for powder X-ray diffraction (XRD) analysis using MiniFlex 600 (Rigaku, CuKα, 40 kV, 15 mA, Tokyo, Japan) at the wavelength of 0.154 nm. A dried synthesized EG-AgNPs was subjected to the scanning electron microscope (JSM-7600F as thermal FESEM, Japan) at 20 kV to study the morphological features of synthesized silver nanoparticles. The metal particles become electronically coupled and aggregated over the time of drying, and it is difficult to find the domain of isolated nanoparticles.

To break the aggregated particles, the dried sample was subjected to probe sonication for a sufficient amount time and the smear was made on a carbon-coated copper grid.

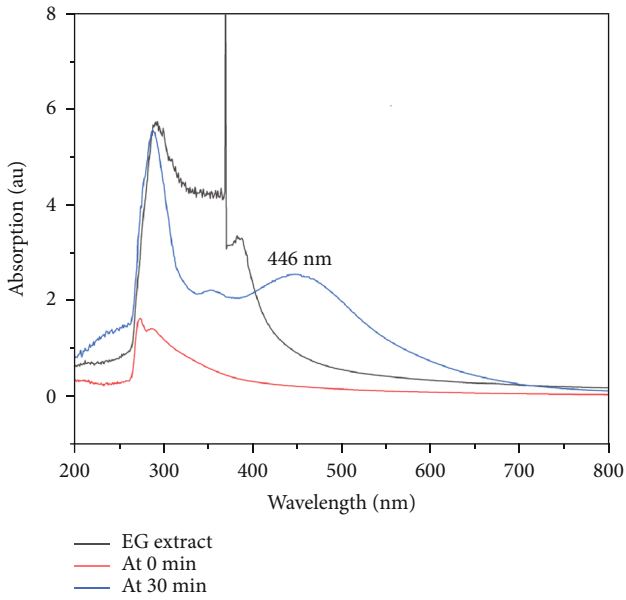

Figure 3: Absorption spectra of the synthesized of biogenic EG-AgNPs.

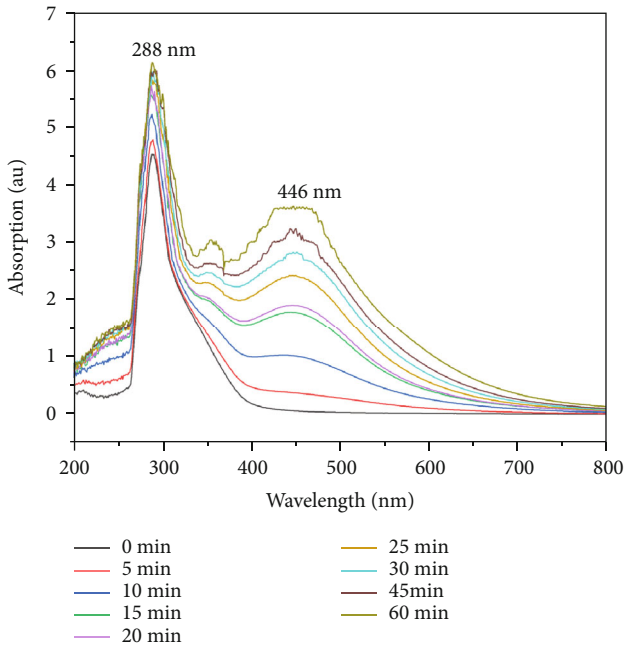

Figure 4: Formation of biomaterials capped AgNPs (EG-AgNPs) with time at 50°C temperature.

The coated film on the SEM grid was allowed to dry under vacuum and exposed 5 min under mercury light. Total composition of elements and atomic proportions of synthesized EG-AgNPs was determined using EDX spectrometer. Nanodimensional morphology of AgNPs was characterized using well-known technique called high-resolution transmission electron microscopy (HRTEM). The synthesized EG-AgNPs were dispersed in milli-Q water and the drop coated in a copper grid, and the micrograph was recorded at an accelerating voltage of 200 kV using HRTEM, JEM-2100F, Japan.

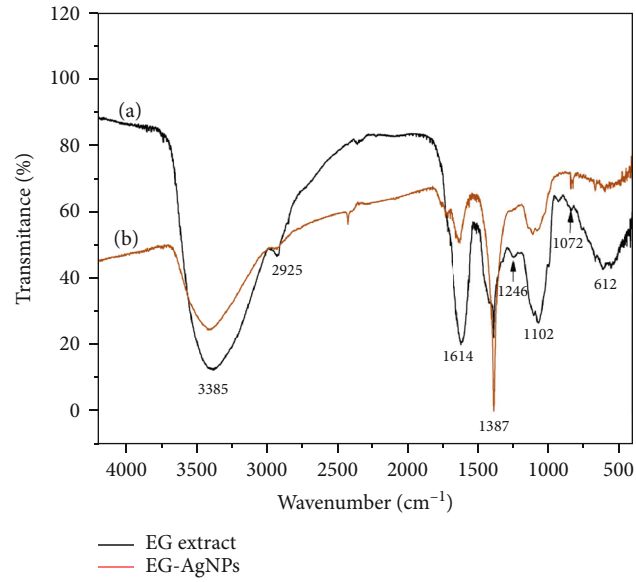

Figure 5: FTIR spectra of the (a) EG extract and (b) EG-AgNPs.

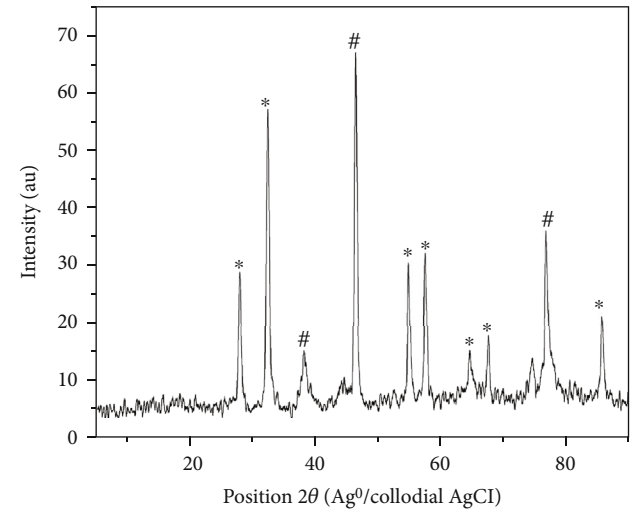

Figure 6: XRD spectrum of synthesized EG-AgNPs.

3.2. Phytochemicals Analysis of E. granulata Extracts. The quantitative analysis of photochemical composition of the *E. granulata* plant extract is given in Figure 2, and also, the qualitative screening is presented in Table 1. The analysis shows that the plant extract has various phytoconstituents such as flavonoids, tannins, and phenolic compounds, glycoside, and proteins. It is noteworthy that the wide spread weed *E. granulata* is showing an interesting and valuable medicinal plant for the therapeutic uses and phytochemical investigations. As per the hypothetical mechanism of biosynthesis of EG-AgNPs, there could be involvement of adequate complex antioxidant enzyme networks [20]. The current investigation result of the antioxidant potential of *E. granulata* extract offers a favorable report toward a hypothetical mechanism about the involvement of antioxidant

Table 2: Observed diffraction peak position and intensity of dried EG-AgNP powder XRD pattern.

X axis	27.88	32.38	38.22	46.36	54.94	57.58	64.62	67.62	74.60	76.84	85.70
Y axis	28.76	57.14	14.92	67.04	30.50	32.01	14.78	17.58	13.57	36.01	20.93
Plane	(111)	(200)	(111)	(220)	(311)	(222)	(220)	(400)	(112)	(311)	(222)

molecules of the plant extract in the biogenic synthesis of silver nanoparticles.

3.3. Synthesis and UV Absorption Analysis of Biogenic EG-AgNPs. Initially, for an adequate test [21], three samples of 9 mL of 1 mM $AgNO_3$ solution were taken as the initial amount to which 1 mL of aqueous leaf extract in each samples was added and incubated at 40°C, 50°C, and 60°C using water both. Over the period of 5 to 10 min, samples at 50°C and 60°C, a visible color change was observed from white to pale yellow, light brown, and then dark brown. The similar changes were observed of sample with 40°C from 15 min onwards. The intensity of the color was increased with increase in incubation time. In the present study, we observed the appearance of the absorption peak at 446 nm which is exactly synchronized with the literature reports. In addition, the formation of EG-AgNPs at room temperature needs a minimum 6 h incubation time. In our study, the observed absorption peak at 446 nm further confirms the biosynthesis of Ag nanoparticles. Figure 3 shows the UV absorption spectra of bioextract (EG), absence of nanoparticle at the time of EG addition in the $AgNO_3$ solution, and the complete formation of EG-AgNP absorption (446 nm) at 50°C.

With the result of stabilized reaction condition for synthesis of biogenic AgNPs in hand, 5 mL of freshly prepared *E. granulata* plant extract was assorted drop wise to 95 mL of 1 mmol aqueous $AgNO_3$ (99.99%) solution. The reaction mixture was kept undisturbed at 50°C until the colorless solution turns to a brownish color. The reaction mixture was turned light brownish color to dark brown color indicates the complete formation of Ag^0 nanoparticles from Ag^+ ions. Synthesized silver nanoparticles were confirmed by sampling the reaction mixture at regular time intervals, and the absorption maxima were recorded by UV/Vis spectra, at the wavelength of 200–800 nm in UV-3600 Shimadzu spectrophotometer at 1 nm resolution [22].

The optical properties of nanoparticles due to collective oscillation of conduction electrons combined with the incident light exhibit strong absorption of electromagnetic wave in the visible region. So, UV-Vis spectroscopy is one of the widely used characterization to understand the formation of nanoparticles. The insight of UV spectra analysis can give the size and shape of the nanoparticles. The complete formation of nanoparticles was observed by UV spectra recorded from reaction mixture at constant time interval of the reaction progress of 0 min to 30 min, and the increased intensity of absorption evidenced that the formation of number of AgNPs in the reaction (Figure 4). The synthesized EG-AgNPs show strong absorption band around 446 nm, which is a typical absorption band of spherical AgNPs due to their surface plasma. Also, the broad absorption band represented that the particles were polydispersed. Over the time of 1 h at 50°C, the smooth absorption peak turns pulse-like band due to the aggregation of generated nanoparticles under applied temperature. Also, there a strong and sharp gradually increasing absorption at 288 nm indicates the increase in concentration of aromatic quinones due to the oxidation of phenolic components in *E. granulata* extraction. The particles were then purified using ultracentrifugation in 20,000 rpm for 20 min. The resulting colloidal precipitate was washed repeatedly in deionized water in order to remove excess silver ions. The purified wet EG-AgNPs were further kept overnight in 60°C in a vacuum oven, and the resulting dried, free flow AgNPs were utilized for further studies.

3.4. Functional Group Analysis of EG-AgNPs. The FTIR spectra of the EG-AgNPs explained the involvement of various aromatic OH compounds in silver nitrate salt reduction and the AgNPs stabilizations [23]. Figure 5(a) represents FTIR spectrum of EG extract with a band at 3385 cm^{-1} corresponds to O-H stretching hydrogen bonded phenols and alcohols. The absorption band 2925 cm^{-1} and 612 cm^{-1} corresponds to C-H stretching vibrations of aromatic and alkyl functional groups, respectively, and the peaks observed at 1614 cm^{-1} represent the presence of intramolecular hydrogen bonded carbonyl keto groups. The sharp band at 1387 cm^{-1} could possibly to N-O asymmetric shows the availability of nitro compounds in the *E. granulata* extract. A band observed at 1072 cm^{-1} could be an aliphatic amines C-N stretching frequency. All aforementioned characteristic functional groups of the phytoconstituents were present in the EG extract, which participates in the bioreduction process for the reduction of silver ion to Ag^0 nanoparticle. The synthesized EG-AgNPs show (Figure 5(b)) lower-intensity FTIR bands at 3392 cm^{-1} than 3385 cm-1 from EG extract, and the aromatic C-H stretching band 2928 cm^{-1} disappeared. Also, the disappearance of fingerprint region bands at ~612 cm^{-1} in EG-AgNPs was observed compared with EG extract. These notable changes presumably indicate the reduction of silver ions (Ag^+) into metallic silver (Ag^0) nanoparticles [24]. The intensity of alkene group 1614 cm^{-1} and alkyl functional groups around 612 cm^{-1} bands reduced indicating the capping effect of the phytocomponents in EG-AgNPs. Also, an intense band appeared at 1387 cm^{-1} shows that nitro compounds in *E. granulata* extract does not involved in the metal ion reduction process. On the other hand, the reduced intensity band at 1072 cm^{-1} shows that the participation of the amine group in the reduction process. It is articulated from the spectrum (Figure 5) that the functional groups present in the *E. granulata* extract involved during the metal ion reduction and certain common functional groups presented in the yielded EG-AgNPs were adsorbed components from the *E. granulata* extract.

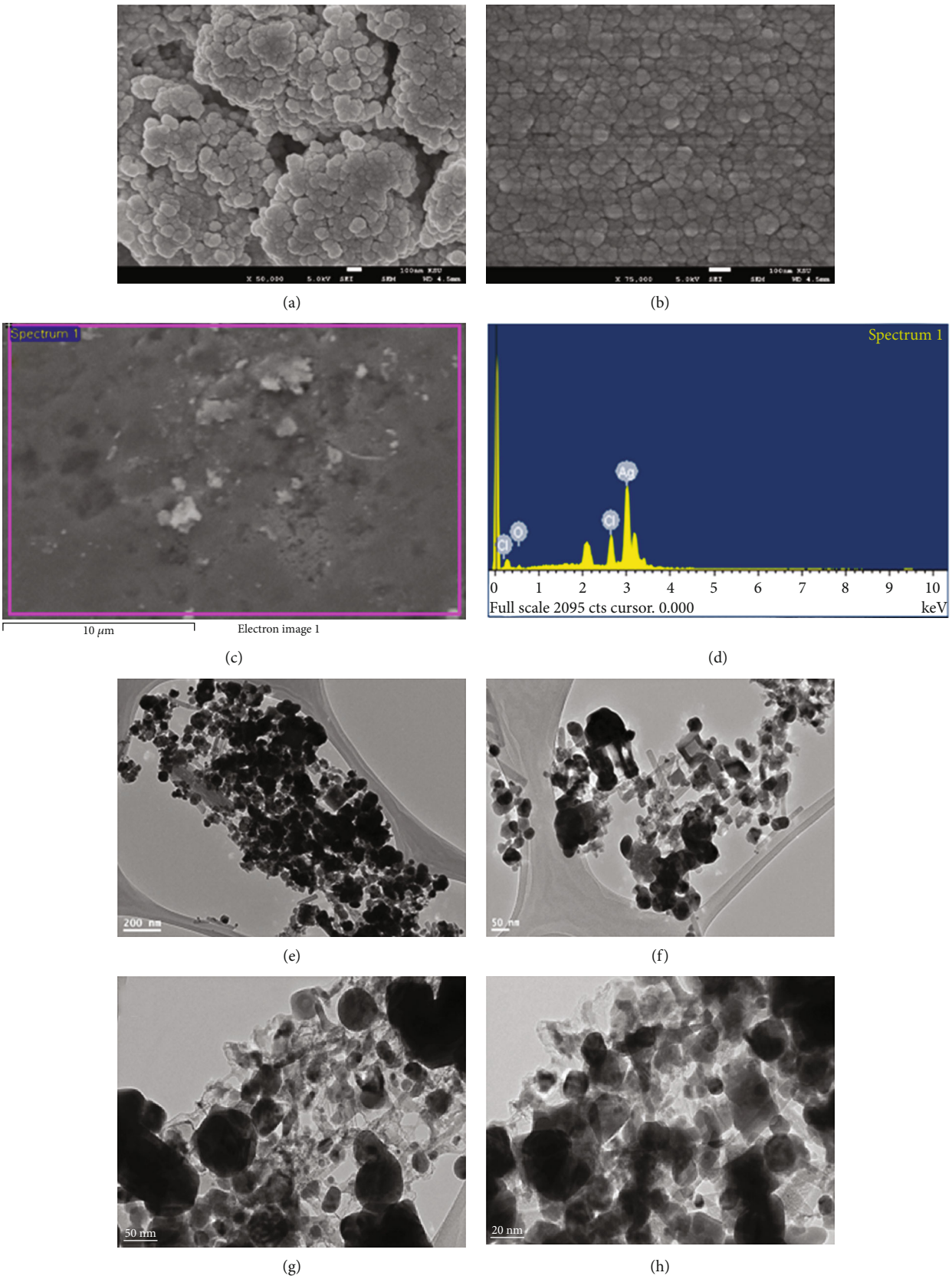

Figure 7: Continued.

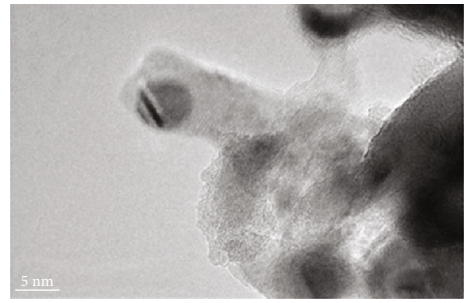

(i)

Figure 7: High-resolution scanning electron microscope (FESEM) images at magnifications: (a) 50000x and (6b) 75000x, energy-dispersive X-ray (EDX) elemental mapping (c), and spectrum of biosorbed Ag/AgCl NPs (d). Transmission electron microscope (TEM) images (e–i).

Table 3: Antimicrobial activity of *E. granulata* extract, EG-AgNPs, and standard drug by an agar well diffusion method.

Microbial pathogens	Zone of inhibition (mm)/concentrations (μg/mL)					
	EG-AgNPs				Plant extract	Ciprofloxacin
	15.00	25.00	50.00	75.00	50.00	10.00
Bacterial pathogens						
S. aureus	7.20 ± 0.60	12.70 ± 0.35	15.40 ± 0.50	17.20 ± 1.30	08.35 ± 1.57	18.95 ± 1.25
E. coli	8.60 ± 2.00	13.40 ± 1.75	15.80 ± 1.15	20.05 ± 0.90	11.38 ± 0.70	21.30 ± 1.65
P. aeruginosa	7.50 ± 0.50	12.18 ± 1.05	15.10 ± 0.63	17.70 ± 1.20	12.50 ± 2.15	18.50 ± 0.55
K. pneumoniae	7.10 ± 0.18	11.70 ± 1.20	16.24 ± 0.48	17.00 ± 1.30	11.73 ± 0.80	17.90 ± 2.40
L. monocytogenes	ND *	07.75 ± 1.70	11.00 ± 0.65	14.05 ± 1.28	13.33 ± 1.52	19.40 ± 0.67
E. faecalis	7.05 ± 1.20	11.95 ± 1.15	16.15 ± 0.45	18.75 ± 0.80	10.55 ± 2.00	19.50 ± 0.52
Fungal pathogens						Amphotericin
C. albicans	8.00 ± 1.15	11.45 ± 1.00	14.66 ± 1.52	16.30 ± 1.05	12.20 ± 2.51	19.40 ± 0.75
Cryptococcus sp.	ND	07.24 ± 0.70	11.15 ± 0.51	13.40 ± 1.25	10.55 ± 0.80	16.25 ± 0.60

*ND: not detected.

Table 4: MIC value of EG-AgNPs by a microdilution method.

Microbial pathogens	MBC value (μg/mL)	
	EG-AgNPs	Ciprofloxacin
Bacterial pathogens		
S. aureus	12.48	3.12
E. coli	6.24	3.12
P. aeruginosa	25.00	6.24
K. pneumoniae	12.48	3.12
L. monocytogenes	≥100.00	6.24
E. faecalis	12.48	6.24
Fungal pathogens		Amphotericin
C. albicans	6.24	6.24
Cryptococcus sp.	12.48	12.48

3.5. Powder X-Ray Diffraction (XRD) Analysis. The crystallinity and mean particle phases of synthesized EG-AgNPs have been characterized using powder XRD pattern (Figure 6). The face centered cubit (FCC) crystalline nature of silver nanoparticles is confirmed based on the observed de Bragg's reflections of dried AgNPs obtained from the biosorbed sample. The peaks appearing position at $2\theta = 38.1, 44.3, 64.4, 77.3$, and 81.5 corresponds to the refractive planes (111), (200), (220), (311), and (222). In comparison to the flection plans, the intensity of the reflection (111) indicates the growth direction of other four nanocrystals. The presence of other reflection peaks may attribute due the presence of colloidal AgCl crystals along with EG-AgNPs. From XRD peaks, utilizing full-width at half-maximum (FWHM) of Gaussian, the average particles' crystallite size was calculated. The FWHM values were applied in the Scherrer equation:

$$D = \frac{k\lambda}{\beta \cos \theta}, \tag{5}$$

where D is the average crystallite size, λ is the X-ray wavelength (CuKα radiation 1.54056 Å), β is line broadening at FWHM in radians, θ is Bragg's angle in degree, and k is the Scherrer constant. The observed values is 0.9438 shows that the synthesized particles are spherical crystals with cubic

symmetry, and the calculated average NP size is about 10.85 nm. The calculated Gaussian fitted FWHM values of EG-AgNPs and EG-AgNPs/AgCl colloids are presented in Table 2 and supporting information (SI) file.[¥]

3.6. Scanning Electron Microscopy (SEM) and Energy-Dispersive X-Ray Spectroscopy (EDX). The FESEM image of the sample was presented in Figures 7(a) and 7(b). The resolution of SEM was operated between a few nanometers to micrometers and at various magnifications which was be easily adjusted. The FESEM micrographs of nanoparticle images showed that the nanoparticles synthesized were polydispersed and most of them are spherical shaped, highly distributed and adsorbed with *E. granulata* biomaterials. Figures 7(c) and 7(d) shows the FESEM-EDX elemental mapping of EG-AgNPs of intense peaks between 2.0 eV and 7.0 eV with 82% of Ag, 9% of oxides, and 8% of chlorine ions. The strong signal of the optical absorbance band at 5.0 eV reveals the presence of pure metallic silver nanoparticles. The presence of other elements signals such that oxygen and chloride ions along with silver ion in the EDX graph explained the presence of colloidal AgCl and binding of the biomolecules to the surface of silver particles. Also, absence of other element signals is the strong evident of the purity of the synthesized EG-AgNPs.

3.7. Transmission Electron Microscopy (TEM) Study. TEM technique involves irradiation of a tiny amount of sample by a high-energy electron beam. As a result, we can obtain clear images of atomic resolution can be visualized for structural characterization and identification of various phases of nanomaterials like, cubic, spherical, or, hexagonal. TEM microscopic analysis (Figures 7(e)–7(i)) of synthesized EG-AgNPs confirmed that most of the nanoparticles were spherical in shape and the size between 5 nm and 30 nm. Also, there are some needle shape particles existing with 5 nm width and 20 nm length. The recorded SEM and TEM images were presented in SI file[¥]. From the results, the synthesized nanoparticles were between 5 nm and 20 nm in size and the mean particle size has been estimated as 15 nm. Also, it shows that nanoparticles were capped with plant constituents which will be very useful to prevent the nanoparticle aggregation.

3.8. Antimicrobial Activity of EG-AgNPs. The antibacterial efficacy of EG-AgNPs was examined for six bacterial pathogenic strains i.e., *S. aureus*, *E. coli*, *L. monocytogenes*, *P. aeruginosa*, *K. pneumoniae*, and *E. faecalis* and two fungal pathogens (*C. albicans* and *Cryptococcus* sp.). The acquired results exhibited that biosynthesized EG-AgNPs demonstrated a significant antimicrobial activity towards all the tested pathogenic strains. The inhibition zones were range between 7.05 ± 1.20 and 21.30 ± 1.65 mm. Inhibition zone results were provided in Table 3. The results presented in Table 3 displayed that the EG-AgNPs efficiently inhibit the growth of tested microbial pathogens to various inhibition zones expect *L. monocytogenes* and *Cryptococcus* sp., from lower to higher concentrations. The EG-AgNPs exhibited maximum activity against *E. coli* (20.05 ± 0.90 mm) and *C. albicans* (16.30 ± 1.05 mm), contrastingly lowest activities found with *L. monocytogenes* (14.05 ± 1.28 mm) and *Cryptococcus* sp. (13.40 ± 1.25), both bacterial and fungal pathogens, respectively. Overall, the antimicrobial activities of EG-AgNPs were maximum and minimum against *E. coli* (bacterial pathogen) and *Cryptococcus* sp. (fungal pathogen), respectively. Further, when compared to standard drug ciprofloxacin (10 μg/mL), EG-AgNPs presented equivalent activities against tested bacterial pathogens than the fungal pathogens.

Table 5: MBC value of EG-AgNPs.

Microbial pathogens	MIC value (μg/mL)	
	EG-AgNPs	Ciprofloxacin
Bacterial pathogens		
S. aureus	6.24	3.12
E. coli	6.24	3.12
P. aeruginosa	25.00	6.24
K. pneumoniae	12.48	3.12
L. monocytogenes	100.00	12.48
E. faecalis	50.00	6.24
Fungal pathogens		Amphotericin
C. albicans	12.48	6.24
Cryptococcus sp.	25.00	12.48

3.9. MIC and MBC of Synthesized EG-AgNPs. EG-AgNPs were found to be a potent antimicrobial activity against both bacterial and fungal pathogens. The documented MIC values of EG-AgNPs on microbial pathogens were presented in Table 4. The results evidently showed that EG-AgNPs efficiently controlled the bacterial growth and also killed the pathogens at low concentrations. The MIC value of EG-AgNPs was minimum (6.24 μg/mL) and maximum (100.00 μg/mL) against tested microbial pathogens. Further, *S. aureus* and *E. coli* were found to be most susceptible pathogens with MIC value of 6.24 μg/mL, whereas *L. monocytogenes* (100.00 μg/mL) considered highly resistant pathogens among the tested bacterial pathogens. Hence, no definite recognized standards for MIC breakpoints on the resistance levels of drugs.

The MBCs are the lowest concentration of any compound that kills the bacterial population at 100%, and it is evident with visible growth of microbial pathogens on agar plates. The MBC values of tested microbial pathogens were presented in Table 5. The minimum and maximum MBC values were found to be 6.24 and $\geq$100.00 μg/mL against *E. coli* and *L. monocytogenes*, respectively. These MBC values are constantly with results of MIC by which *E. coli* was viewed as the most susceptible pathogens. The observed MIC and MBC petri plate images were presented in SI file[¥].

Generally, AgNPs are extensively used in the pharmaceutical industry and it has potential inhibitory activities against various microorganisms. It has also been used as an ointment to subside the microbial infections particularly from burns and wounds without cytotoxicity [25, 26]. Hence, the present study results encouraged and revealed one more effective and efficient plant extract-mediated silver nanoparticles with more promising biological applications in future therapeutic approaches.

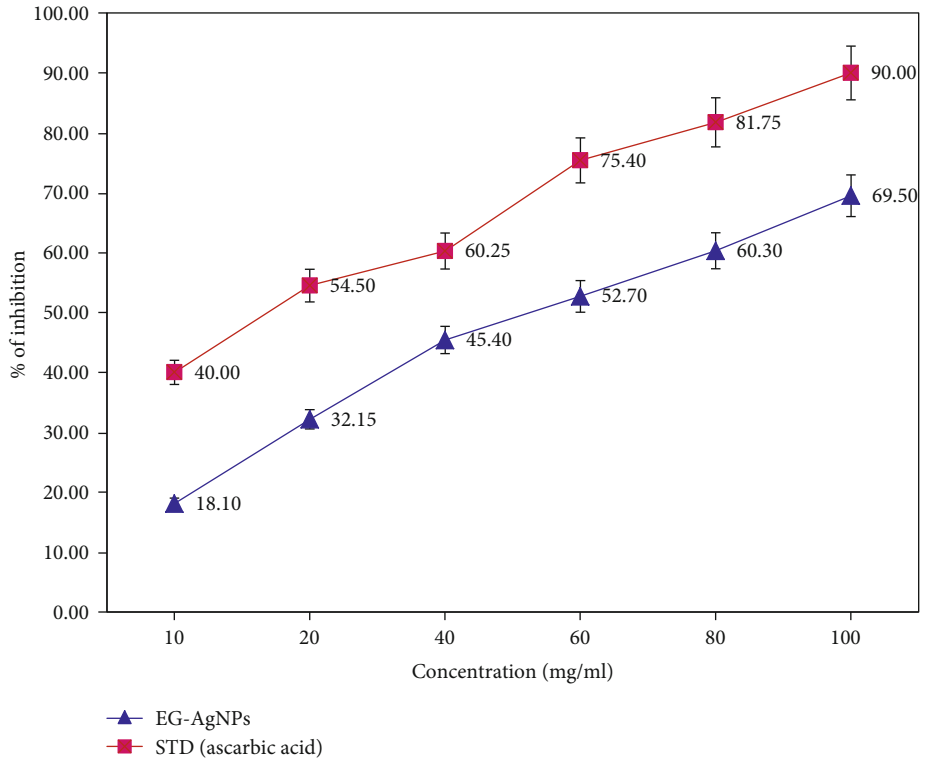

Figure 8: Radical scavenging activity of EG-AgNPs.

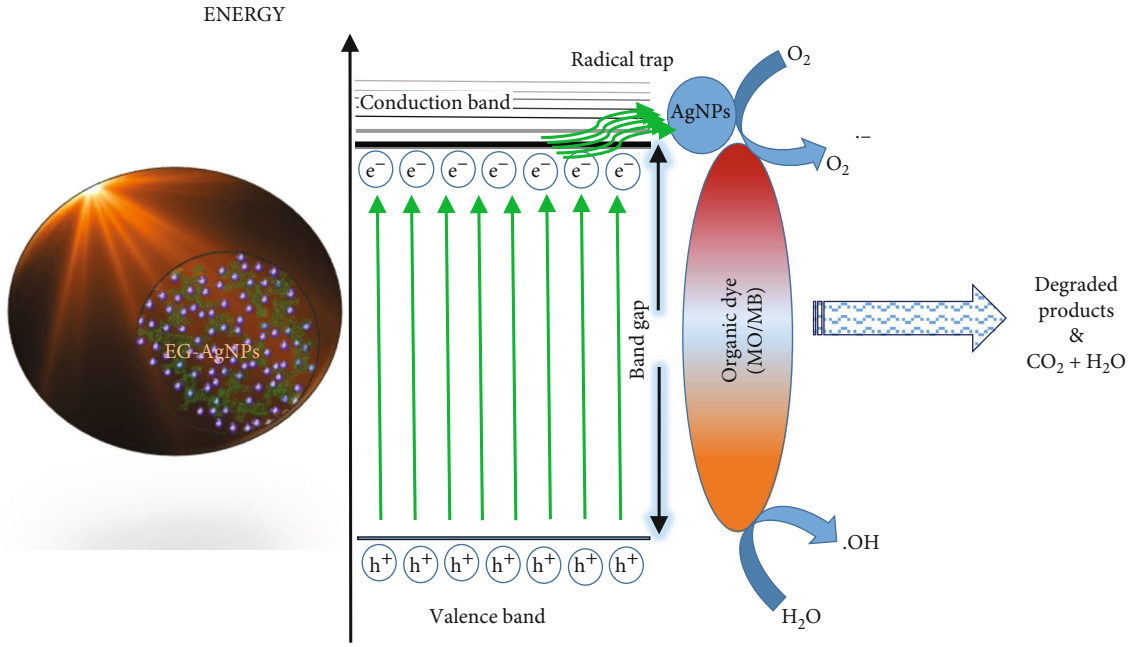

Figure 9: Schematic diagram of the mechanism of EG-AgNPs catalyzed dye degradation.

3.10. Radical Scavenging Activity of EG-AgNPs by DPPH Method. The significant antioxidant potential of EG-AgNPs was evaluated by DPPH radical scavenging assay having IC_{50} 30.04 μg/mL (Figure 8). The ascorbic acid was used as a standard. The results strongly recommend the application of EG-AgNPs as useful natural antioxidants for health preservation against different oxidative stress associated with degenerative diseases. In fact, antioxidant evaluation is essential for EG-AgNPs before its use in *in vivo* models and also biomedical applications. The current antioxidant activity result correlated

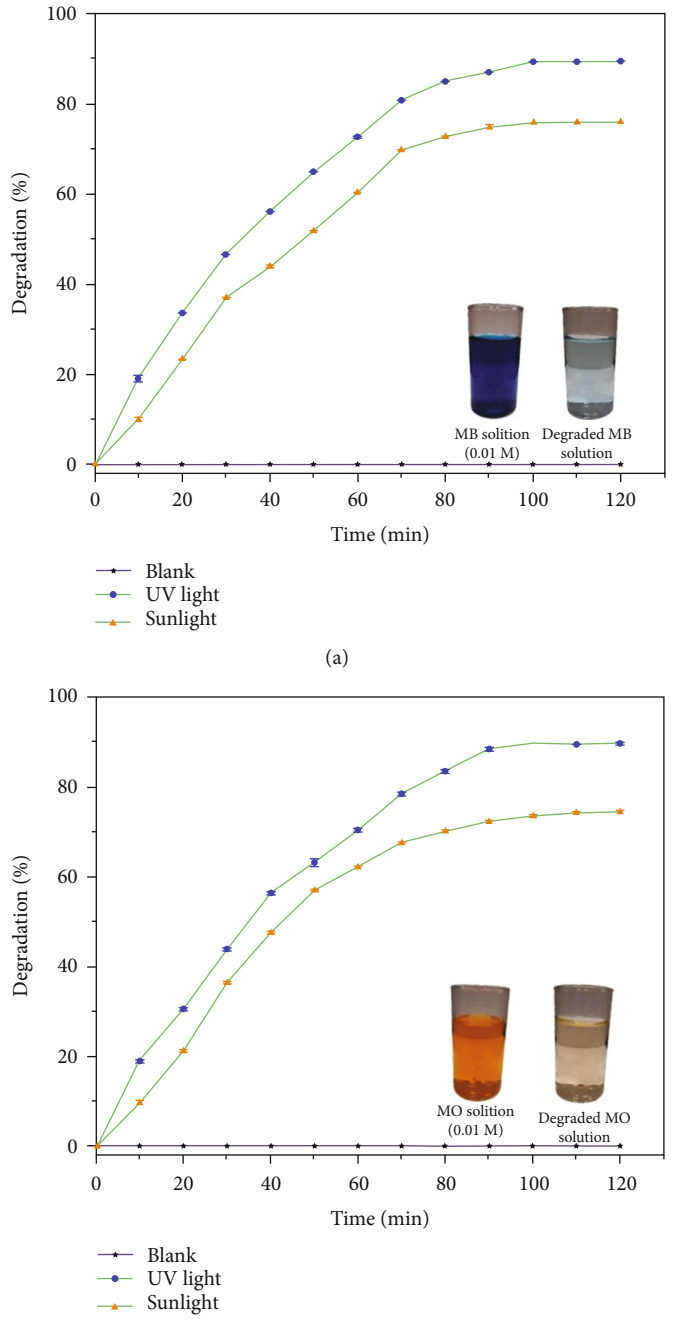

Figure 10: EG-AgNPs supported photocatalytic degradation of (a) MB and (b) MO dyes at various time periods under UV and sunlight irradiation.

with a previous report evaluated by literature reports [27]; they investigated *in vitro* antioxidant activity of biosynthesized nanoparticles from *P. pinnata* extract and found significant free radical scavenging potential.

Mostly, AgNPs are extensively used in the pharmaceutical industry and it has potential inhibitory activities against various microorganisms. It also been used as an ointment to subsides the microbial infections particularly from burns and wounds. Hence, the present study results encouraged and revealed one more effective and efficient plant extract mediated silver nanoparticles with more promising biological applications in future therapeutic approaches.

3.11. Catalytic Activity towards MB and MB Degradation. The general photocatalytic performance was taken under UV irradiation due to the presence of potential energy barrier between the valance band and conduction band. The organic dye undergoes irradiation of incident light electron are excited from the valance band to conduction band. Having EG-AgNPs in the reaction mixture, the silver nanoparticles are readily accepting

the excited state electron and it presents the recombination of electron with valance band holes. Therefore, the valance band positively charged holes interact with H_2O and producing OH radicals ($^{\cdot}OH$). At the same time, the excited state electrons present in silver nanoparticles produces superoxide radical anions ($O_2^{\cdot-}$) by reacting with oxygen, which also react with H_2O and generated OH radicals. These generated superoxide and OH radicals undergo reaction with dye molecule and produce H_2O and CO_2. The overall degradation process is schematically represented in Figure 9.

Figure 10 shows that EG-AgNPs' supported degradation process was effectively done both under sunlight and UV light irradiation, and at the same time, there is no notable dye degradation observed in the blank solutions. Though the dye degradation is carried out in both sunlight and UV light, the UV irradiation works efficiently for degrading dyes in the presence of EG-AgNPs.

Figure 10(a) shows that the degradation of MO is about 89.91% and 72.02% under UV light and sunlight, respectively. Likewise, Figure 10(b) shows that MB degraded about 89.34% and 75.95% under UV light and sunlight irradiation, respectively. Both MO and MB dyes are degraded almost equally, and the little bit higher degradation nature of cationic dye MB may be due to the presence of the positively charged vacant sulfur group. The observed triplicate values of both MO and MB dye degradation were presented in SI file¥.

4. Conclusions

In this study, we have achieved to synthesize biogenic AgNPs (EG-AgNPs) using E. granulata plant extract as reductant at 50°C in neutral pH and without using any harmful reducing agents. The formation of EG-AgNPs was confirmed through UV-VIS, FTIR, and XRD spectroscopies and electron microscopic analysis. The morphology and shape of EG-AgNPs were confirmed by HRSEM, and the particles are spherical, rod, and needle with 5 to 20 nm in size has been identified by HRTEM analysis. The EG-AgNPs showed antioxidant and excellent antimicrobial activities against various pathogenic microorganisms. Among the tested pathogens, S. aureus and E. coli were found to be the most susceptible pathogens with MIC value of 6.24 μg/mL whereas, L. monocytogenes (100.00 μg/mL) are considered highly resistant pathogens among the tested bacterial pathogens. Also, EG-AgNPs have the ability for free radical scavenging and more than 85% of toxic organic dye degradation. Based on the aforementioned results, the synthesized EG-AgNPs are fascinating and suitable for upscaling of metallic organonanomaterials to explore various biomedical as well as catalytic applications.

Data Availability

Recorded SEM, TEM, and XRD data and antibacterial growth inhibition images of synthetized EG-AgNPs were available in electronic supplementary information.

Conflicts of Interest

The authors declare that they have no conflicts of interest.

Acknowledgments

The authors acknowledge the King Saud University, Riyadh, Saudi Arabia, for funding this work through Researchers Supporting Project number (RSP-2021/30).

Supplementary Materials

Recorded SEM, TEM, and XRD data and antibacterial growth inhibition images of synthetized EG-AgNPs were available in the electronic supplementary information. *(Supplementary Materials)*

References

[1] M. Kaur and D. S. Chopra, "Green synthesis of iron nanoparticles for biomedical applications," *Global Journal of Nanomedicine*, vol. 4, no. 4, pp. 1–10, 2018.

[2] J. Helmlinger, C. Sengstock, C. Groß-Heitfeld et al., "Silver nanoparticles with different size and shape: equal cytotoxicity, but different antibacterial effects," *RSC Advances*, vol. 6, no. 22, pp. 18490–18501, 2016.

[3] L. Boselli, H. Lopez, W. Zhang et al., "Classification and biological identity of complex nano shapes," *Communications Materials*, vol. 1, no. 1, 2020.

[4] R. Ridolfo, S. Tavakoli, V. Junnuthula, D. S. Williams, A. Urtti, and J. C. M. Van Hest, "Exploring the impact of morphology on the properties of biodegradable nanoparticles and their diffusion in complex biological medium," *Biomacromolecules*, vol. 22, no. 1, pp. 126–133, 2021.

[5] M. A. Raza, Z. Kanwal, A. Rauf, A. N. Sabri, S. Riaz, and S. Naseem, "Size- and shape-dependent antibacterial studies of silver nanoparticles synthesized by wet chemical routes," *Nanomaterials*, vol. 6, no. 4, 2016.

[6] N. Jain, A. Bhargava, S. Majumdar, J. C. Tarafdar, and J. Panwar, "Extracellular biosynthesis and characterization of silver nanoparticles using Aspergillus flavus NJP08: a mechanism perspective," *Nanoscale*, vol. 3, no. 2, pp. 635–641, 2011.

[7] L. Wang, G. Periyasami, A. Aldalbahi, and V. Fogliano, "The antimicrobial activity of silver nanoparticles biocomposite films depends on the silver ions release behaviour," *Food Chemistry*, vol. 359, article 129859, 2021.

[8] M. Ovais, A. T. Khalil, A. Raza et al., "Green synthesis of silver nanoparticles via plant extracts: beginning a new era in cancer theranostics," *Nanomedicine*, vol. 11, no. 23, pp. 3157–3177, 2016.

[9] F. Rodríguez-Félix, A. G. López-Cota, M. J. Moreno-Vásquez et al., "Sustainable-green synthesis of silver nanoparticles using safflower (Carthamus tinctorius L.) waste extract and its antibacterial activity," *Heliyon*, vol. 7, no. 4, p. e06923, 2021.

[10] C. V. Restrepo and C. C. Villa, "Synthesis of silver nanoparticles, influence of capping agents, and dependence on size and shape: a review," *Environmental Nanotechnology, Monitoring and Management*, vol. 15, 2021.

[11] G. Bagalkotkar, S. R. Sagineedu, M. S. Saad, and J. Stanslas, "Phytochemicals from Phyllanthus niruri Linn. and their pharmacological properties: a review," *Journal of Pharmacy and Pharmacology*, vol. 58, no. 12, pp. 1559–1570, 2010.

[12] B. K. Ghimire, J.-W. Seo, S.-H. Kim et al., "Influence of harvesting time on phenolic and mineral profiles and their

association with the antioxidant and cytotoxic effects of Atractylodes japonica Koidz," *Agronomy*, vol. 11, no. 7, 2021.

[13] L. M. Ndam, A. M. Mih, A. S. Tening, A. G. N. Fongod, N. A. Temenu, and Y. Fujii, "Phytochemical analysis, antimicrobial and antioxidant activities of Euphorbia golondrina L.C. Wheeler (Euphorbiaceae Juss.): an unexplored medicinal herb reported from Cameroon," *SpringerPlus*, vol. 5, no. 1, 2016.

[14] E. A. Ainsworth and K. M. Gillespie, "Estimation of total phenolic content and other oxidation substrates in plant tissues using Folin-Ciocalteu reagent," *Nature Protocols*, vol. 2, no. 4, pp. 875–877, 2007.

[15] P. Kalita, B. K. Tapan, T. K. Pal, and R. Kalita, "Estimation of total flavonoids content (Tfc) and anti oxidant activities of methanolic whole plant extract of Biophytum sensitivum Linn," *Journal of Drug Delivery and Therapeutics*, vol. 3, no. 4, pp. 33–37, 2013.

[16] S. Magaldi, S. Mata-Essayag, C. H. de Capriles et al., "Well diffusion for antifungal susceptibility testing," *International Journal of Infectious Diseases*, vol. 8, no. 1, pp. 39–45, 2004.

[17] S. Khorrami, A. Zarrabi, M. Khaleghi, M. Danaei, and M. R. Mozafari, "Selective cytotoxicity of green synthesized silver nanoparticles against the MCF-7 tumor cell line and their enhanced antioxidant and antimicrobial properties," *International Journal of Nanomedicine*, vol. Volume 13, pp. 8013–8024, 2018.

[18] O. M. Okawam, J. Kinjo, and T. Nohara, "Atividade de eliminação do radical DPPH (1,1-difenil-2-picrilhidrazil) de flavonóides obtidos de algumas plantas medicinais," *Biological and Pharmaceutical Bulletin*, vol. 24, no. 10, pp. 1202–1205, 2001.

[19] D. Gola, A. Kriti, N. Bhatt et al., "Silver nanoparticles for enhanced dye degradation," *Current Research in Green and Sustainable Chemistry*, vol. 4, article 100132, 2021.

[20] R. Prasad, "Synthesis of silver nanoparticles in photosynthetic plants," *Journal of Nanoparticles*, vol. 2014, 8 pages, 2014.

[21] C. Li, D. Chen, and H. Xiao, "Green synthesis of silver nanoparticles using _Pyrus betulifolia Bunge_ and their antibacterial and antioxidant activity," *Materials Today Communications*, vol. 26, article 102108, 2021.

[22] B. Deeksha, V. Sadanand, N. Hariram, and A. V. Rajulu, "Preparation and properties of cellulose nanocomposite fabrics with in situ generated silver nanoparticles by bioreduction method," *Journal of Bioresources and Bioproducts*, vol. 6, no. 1, pp. 75–81, 2021.

[23] S. Raj, R. Trivedi, and V. Soni, "Biogenic synthesis of silver nanoparticles, characterization and their applications-a review," *Surfaces*, vol. 5, no. 1, pp. 67–90, 2022.

[24] M. S. Niloy, M. M. Hossain, M. Takikawa et al., "Synthesis of biogenic silver nanoparticles using Caesalpinia digyna and investigation of their antimicrobial activity and in vivo biocompatibility," *ACS Applied Bio Materials*, vol. 3, no. 11, pp. 7722–7733, 2020.

[25] B. Boonkaew, P. Suwanpreuksa, L. Cuttle, P. M. Barber, and P. Supaphol, "Hydrogels containing silver nanoparticles for burn wounds show antimicrobial activity without cytotoxicity," *Journal of Applied Polymer Science*, vol. 131, no. 9, pp. 1–10, 2013.

[26] Y. K. Mohanta, S. K. Panda, R. Jayabalan, N. Sharma, A. K. Bastia, and T. K. Mohanta, "Antimicrobial, Antioxidant and Cytotoxic Activity of Silver Nanoparticles Synthesized by Leaf Extract of Erythrina suberosa (Roxb.)," *Frontiers in Molecular Biosciences*, vol. 4, no. 14, pp. 1–9, 2017.

[27] S. H. Priya, N. Prakasan, and J. Purushothaman, "Antioxidant activity, phenolic - flavonoid content and HPLC profiling of three different variants of Syzygium cumini seeds - a comparative study," *Journal of Intercultural Ethnopharmacology*, vol. 6, no. 1, pp. 107–114, 2017.